Mechanical Properties and Fracture Behavior of Polypropylene Reinforced with Polyaniline-Grafted Short Glass Fibers

O. Flores,[1] A. Romo-Uribe,[1] M. E. Romero-Guzmán,[1] A. E. González,[1] R. Cruz-Silva,[2] B. Campillo[1,3]

[1]*Instituto de Ciencias Físicas, Universidad Nacional Autónoma de México, Avenida Universidad s/n Colonia Chamilpa, Cuernavaca Morelos 62210, México*
[2]*Centro de Investigación en Ingeniería y Ciencias Aplicadas, Universidad Autónoma del Estado de Morelos, Cuernavaca Morelos 62210, México*
[3]*Facultad de Química, Universidad Nacional Autónoma de México, Ciudad Universitaria DF 04510, México*

Received 8 April 2008; accepted 8 October 2008
DOI 10.1002/app.29453
Published online 23 January 2009 in Wiley InterScience (www.interscience.wiley.com).

ABSTRACT: This research was focused on the mechanical properties of electrically conducting composites based on polyaniline (PAn)-coated short glass fibers (SGFs) immersed in an isotactic polypropylene (iPP) matrix. In these composites, PAn was actually grafted onto the SGF surface, and so it was denoted PAn-*g*-SGF. The tensile, flexural, and interlaminar fracture toughness was investigated. To study the influence of PAn-*g*-SGF, three different concentrations (10, 20, and 30 wt %) were melt-mixed in the iPP resin with a batch mixer. X-ray patterns of the as-molded plaques of iPP and its composites showed an isotropic orientation. Uniaxial tensile deformation revealed that the Young's modulus and tensile stress increased as the concentration of PAn-*g*-SGF increased; on the other hand, the strain at failure was significantly reduced (by 2 orders of magnitude) with respect to the neat iPP. Scanning electron microscopy studies on the failure specimens indicated that the significant reduction of the strain at failure was due to the low interfacial bonding between the fibers and the surrounding matrix. Moreover, X-ray scattering analyses of the fractured regions showed that the uniaxial deformation enabled significant molecular orientation in the iPP, whereas the fractured composites remained isotropic. Detailed scanning electron microscopy analyses showed that the fracture mechanism arose from the fracture of the PAn-*g*-SGFs; the percolated PAn-*g*-SGFs formed a path for the stress transfer. Because the failure was dominated by both filler decohesion and polymeric chain rupture, the strength was not influenced significantly by the amount of PAn-*g*-SGFs. J Appl Polym Sci 112: 934–941, 2009

Key words: composites; conducting polymers; fracture; mechanical properties

INTRODUCTION

Many new possibilities have been revealed by the production of intrinsically conductive polymers, such as protection from direct electrostatic discharge (ESD) and, in general, electromagnetic interference field (EMI) shielding. The benefits include weight reduction, physical flexibility, and tunable shielding responses. To use them as dissipative materials for ESD shielding, their electrical conductivity has to be between 10^{-11} and 10^{-4} S/cm (ANSI/EIA-541). Polyaniline (PAn) has been increasingly studied in recent years, being one of the most promising electrically conducting polymers because of its high polymerization yield, good environmental stability combined with moderate electrical conductivity, and relatively low cost.[1–7] However, blends of PAn with thermoplastics usually show decreases in the mechanical properties, and this makes them unsuitable for manufacturing strong devices with the aforementioned ESD and EMI protection properties.

The introduction of reinforcing fibers has long been a remedy in the polymer industry to improve the mechanical properties of different composites. Among them, glass fibers have been shown to be a good reinforcement for the production of materials

Correspondence to: A. Romo-Uribe (aromo-uribe@fis.unam.mx).

Contract grant sponsor: Dirección General de Asuntos del Personal Académico/Programa de Apoyo a Proyectos de Investigación e Inovación Tecnológica (to A.E.G.); contract grant number: IN106008.

Contract grant sponsor: Consejo Nacional de Ciencia y Tecnología (to A.R.-U.); contract grant number: CIAM 2006 58646.

Contract grant sponsor: Dirección General de Asuntos del Personal Académico/Universidad Nacional Autónoma de México (to M.E.R.-G.).

capable of withstanding the stresses in end-use environments because they offer high tensile strength, high Young's modulus, high heat resistance, production from readily available raw materials, and low cost. However, a previous study found that with the incorporation of PAn complexes into a polypropylene (PP) matrix with short glass fibers (SGFs), the mechanical properties actually decreased because of the very poor adhesion of the SGFs with the PP–PAn matrix; this reduced the tensile modulus and tensile strength with respect to the PP–SGF composites.[1]

Recently, a great number of investigations have been carried out on the coating of different materials with intrinsically conductive polymers.[8] For the case of glass surfaces coated with PAn, the coating was usually achieved by simple immersion of the glass substrate into the polymerization solution. Tuning the duration of the substrate dipping varied the thickness of the deposited films. The problem with this method is that poor adhesion of the PAn is obtained when smooth surfaces such as glass are covered. Nevertheless, this problem can be overcome by chemical grafting of the PAn to the glass surface, a procedure pioneered by Wu and coworkers[9,10] and later refined by Li and Ruckenstein.[11] However, these PAn-grafted glass fibers have not been used to prepare fiber-reinforced composites by melt processing techniques.

Cruz-Silva and coworkers[12,13] reported a novel reactor design for the synthesis of PAn-*g*-SGF, and isotactic polypropylene (iPP)/PAn-*g*-SGF composites were prepared by melt compounding. Although the linear viscoelastic properties of molten iPP/PAn-*g*-SGF composites have already been investigated[14] and a superficial investigation of the mechanical properties, mainly the Young's modulus and tensile strength, has been reported for these composites,[12] the purpose of this work is to carry out a detailed study of their mechanical properties and fracture behavior. The mechanical properties are correlated with the microstructure measured via scanning electron microscopy (SEM) and wide-angle X-ray scattering (WAXS). That is, we study not only the Young's modulus and the strength at fracture but also the yield strength, the ultimate tensile strength (UTS), the strain at fracture, and the morphology after deformation. Furthermore, we also investigate and correlate with the microstructure the fracture mechanism, whether it is brittle or ductile.

EXPERIMENTAL

Materials

The preparation of electrically conducting iPP/PAn-*g*-SGF composites and the thermal and electrical properties of iPP/PAn–SGF composites were investigated by Cruz-Silva and coworkers.[12,13] PAn-*g*-SGF was thermally blended with iPP homopolymer (HP423M, Valtec; melt flow index = 3.8, density = 0.9 g/cm^3) [Indelpro, Monterrey, Mexico] in a batch mixer (Plasticorder PL2000, Brabender) [Duisburg, Germany] at 60 rpm for 12 min at 200°C. PP composites with PAn-*g*-SGF concentrations ranging from 10 to 30 wt % were prepared. The resulting composites were compression-molded into plaques 2.6 mm thick at 200°C under 2.45 MPa for 10 min. Table I shows the compositions of the composites.

TABLE I
Compositions of the iPP/PAn-*g*-SGF Composites

Sample	iPP	PAn-*g*-SGF (wt %)
PP00	100	0
PP10	90	10
PP20	80	20
PP30	70	30

Mechanical properties

The influence of PAn-*g*-SGF on the mechanical properties of the composites was studied under uniaxial tension. Compression-molded PPs with and without PAn-*g*-SGF were mechanically tested in accordance with the ASTM D 638 standard.[15] Tension tests were carried out at room temperature on an Instron 4206 (Massachusetts, USA) universal testing machine with a crosshead speed of 5 mm/min.

SEM

The evaluation of the fiber adherence and the fracture mode in the fractured surfaces was carried out with SEM. A JEOL model 6400 scanning electron microscope was used. The sample's fracture surfaces were metal-coated with Au/Pd by a sputtering procedure.

WAXS

Two-dimensional X-ray scattering patterns were collected at the Advanced Photon Source, Argonne National Laboratory (Argonne, IL), on the DuPont–Northwestern–Dow Collaborative Access Team Beamline 5-BM-D. The samples were investigated in transmission mode. A Si (111) double-crystal monochromator was used, whose crystals were detuned with respect to one another with a piezo crystal tilt stage to reduce the amount of harmonics in the Bragg reflected beam. In these experiments, the monochromator was detuned to typically 80% of the maximum of the rocking curve. X-rays of 35 keV collimated to a 1-mm-diameter were used. WAXS patterns were acquired with the Mar 165 (Illinois, USA) charged coupling device detector. An exposure time of 120 s was used to collect each pattern. The

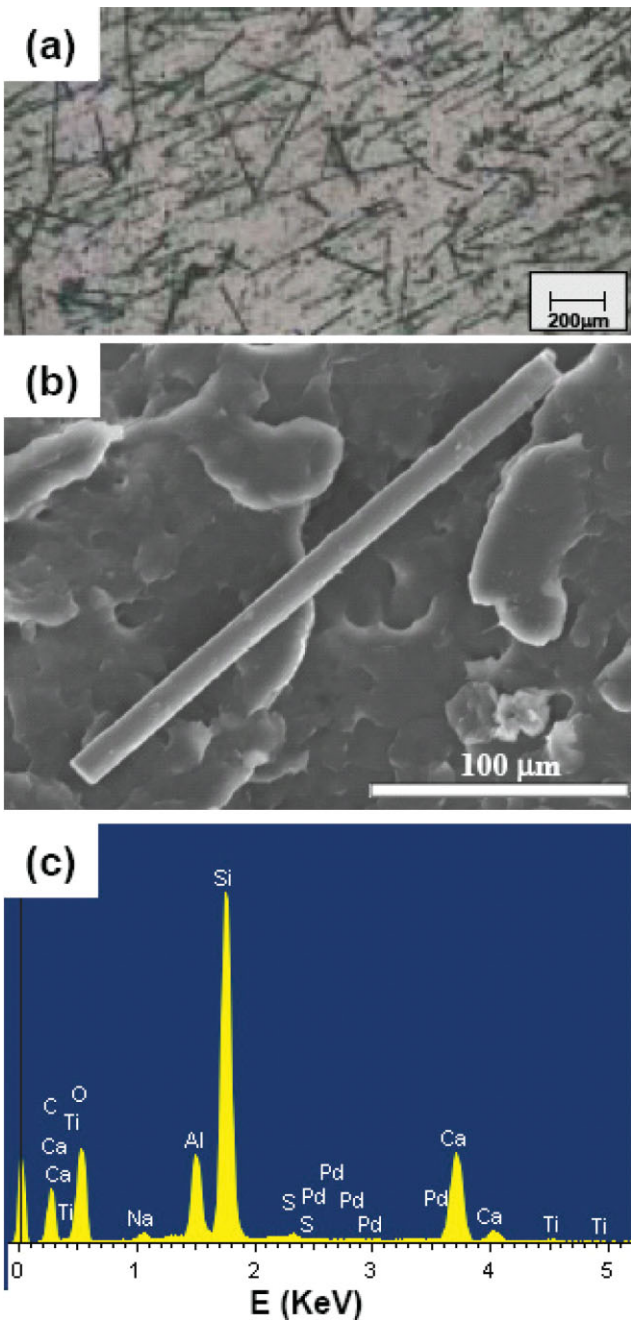

Figure 1 (a) Optical micrograph of the iPP composite with 10 wt % PAn-*g*-SGF under white-light conditions, (b) SEM micrograph of PAn-coated SGF, and (c) elemental analysis of the fiber shown in part b (E = energy). [Color figure can be viewed in the online issue, which is available at www.interscience.wiley.com.]

sample-to-detector distance was 705 mm, and this was calibrated with a silver behenate standard. The X-ray patterns were spatially corrected, and incoherent background scattering was subtracted from each pattern. Data reduction and data analysis were carried out with the Polar version 2.6 software package (Stonybrook Technology and Applied Research, Inc.) [New York, USA].

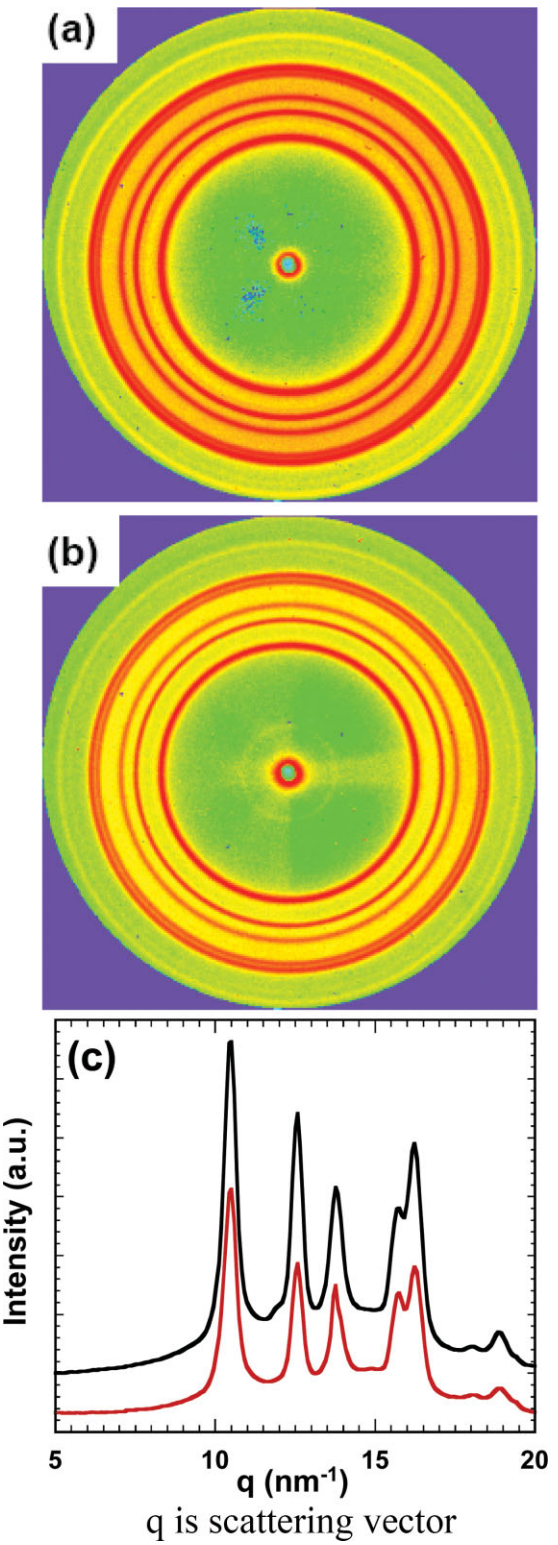

Figure 2 q is scattering vector. (a,b) WAXS patterns of molded sheets of neat PP and the iPP composite containing 10 wt % PAn-*g*-SGF, respectively, and (c) azimuthally averaged radial intensity scans from patterns in parts a and b. [Color figure can be viewed in the online issue, which is available at www.interscience.wiley.com.]

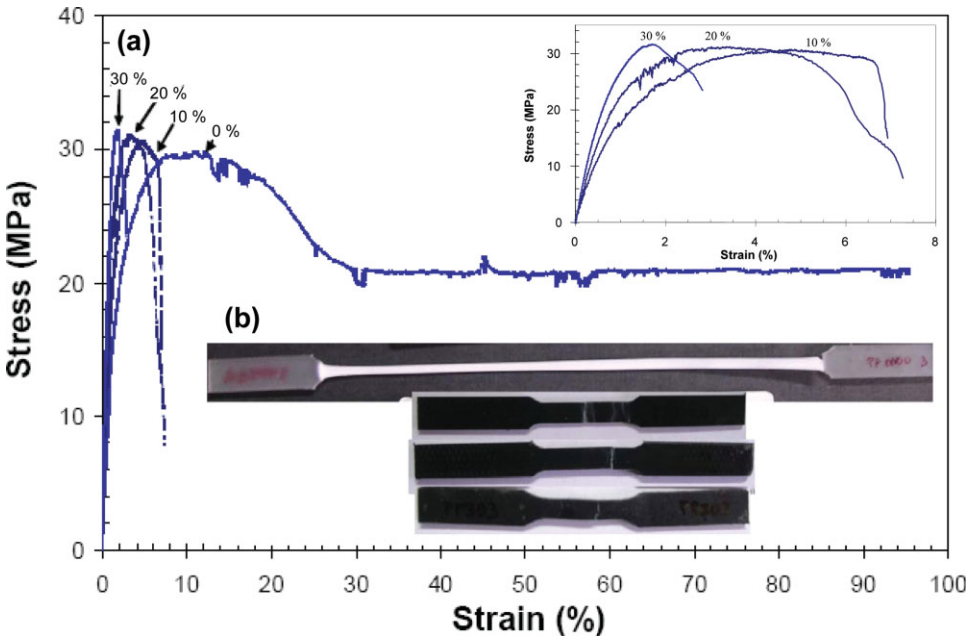

Figure 3 (a) Stress–strain traces of PP and composites containing 10, 20, or 30 wt % PAn-*g*-SGF. The inset graph is an enlargement of the stress–strain traces of the composites. (b) Samples after the uniaxial tension experiment: PP and composites with 10, 20, or 30 wt % PAn-*g*-SGF (from top to bottom). The composites showed vertical white bands associated with the regions of yielding; this was more noticeable in the sample with 10 wt % PAn-*g*-SGF. A strain rate of 5 mm/min was applied at room temperature. [Color figure can be viewed in the online issue, which is available at www.interscience.wiley.com.]

RESULTS AND DISCUSSION

The degree of dispersion of the PAn-*g*-SGFs in the PP matrix was investigated via optical microscopy. Figure 1(a) shows the optical micrograph of sample PP10 containing 10 wt % PAn-*g*-SGF. PAn-*g*-SGF was well dispersed in the polymeric matrix. Figure 1(b) shows an SEM micrograph of a single PAn-*g*-SGF, and it can be seen that the glass fiber was indeed completely coated by the PAn in agreement with previous reports.[13,14] The results of the elemental analysis of a single PAn-*g*-SGF are shown in Figure 1(c); the spectrum shows that the most predominant element was Si.

The microstructure of the as-molded composite plaques was investigated by WAXS. 2D WAXS patterns of PP00 and PP10 are shown in Figure 2(a,b), respectively. The background-corrected patterns show sharp Debye–Scherrer reflections (i.e., sharp in 2θ), which are typical of polycrystalline materials. The crystalline reflections are superimposed on a broad amorphous halo. Figure 2(c) shows the radial scans obtained from these patterns. The scans show that the crystallographic structure of iPP was not affected by the presence of PAn-*g*-SGF. Moreover, the uniform azimuthal intensity of the crystalline reflections observed in the patterns [Figs. 2(a,b)] indicates that there was no preferred molecular orientation in the as-molded plaques.

Figure 3 shows the tensile stress curves for the PP reinforced with PAn-*g*-SGF, and for comparison, the curve for the PP00 sample is also shown. In the case of the composites, it can be observed that the yielding was followed quickly by failure, which indicated the formation of a neck and cracks in the interfaces between the PAn-*g*-SGF and the PP matrix. On the other hand, the curve for the PP00 sample shows a

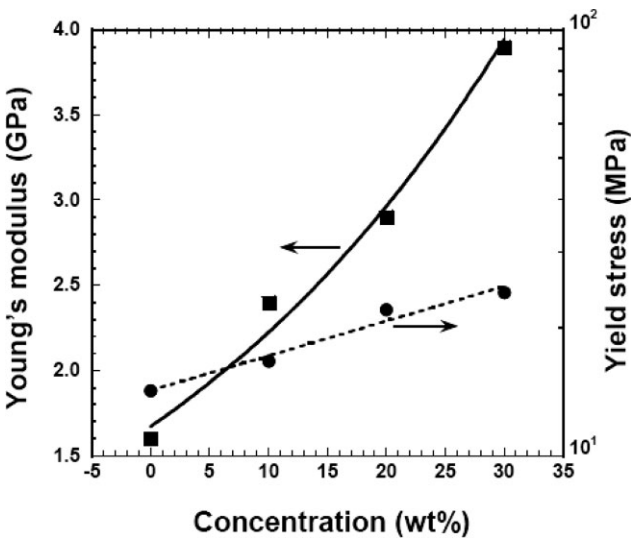

Figure 4 Plot of Young's modulus and the yield stress as a function of the PAn-*g*-SGF concentration.

TABLE II
Mechanical Properties of the iPP/PAn-*g*-SGF Composites Obtained Under Uniaxial Tension at 5 mm/min

Sample	UTS (MPa)	Young's modulus (GPa)	Yield stress (MPa)	Stress at fracture (MPa)	Strain (%)
PP00	29.9	1.6	14.2	20.9	405.6
PP10	30.7	2.4	16.7	14.9	6.9
PP20	31.1	2.9	22.0	7.9	7.3
PP30	31.6	3.9	24.2	22.5	2.9

typical behavior found in several semicrystalline and glassy polymers.[16] There was nonhomogeneous deformation with a stable neck in tension. The neck was formed at a UTS point of 29.9 MPa of stress and 10.1% strain. As the deformation proceeded, there was a reduction in the strength around 21 MPa, at which the neck was stabilized at about 31% strain, and it underwent a reasonable amount of plastic deformation. It is also noted that the stress–strain curve of PP00 did not manifest any strain hardening. During this process (cold drawing), the PP chains were aligned along the stress direction (see the X-ray scattering results later).

The inset plot in Figure 3 shows only the stress–strain curves for the reinforced samples. Serrated behavior can be observed in the stress–strain curves, which may be associated with the fracture of PAn-*g*-SGF and a decohesion process between the PAn-*g*-SGF and the PP matrix. The maximum strain is almost the same for the 10 and 20 wt % PAn-*g*-SGF content samples, but in the case of 30 wt % PAn-*g*-SGF, this value fell to 2.9% strain. This behavior is due to the inhibition of the chain alignment process by the presence of a higher concentration of PAn-*g*-SGF. In Figure 3, we can also observe photographs of the samples after the uniaxial tension experiment. The composites showed vertical white bands associated with the regions of yielding.

Figure 4 shows the Young's modulus and the yield stress as a function of the PAn-*g*-SGF concentration. These results show that both physical properties were enhanced as the concentration of PAn-*g*-SGF was increased. The results of the mechanical properties tests are summarized in Table II. It can be seen that the addition of PAn-*g*-SGF led to a considerable reduction of the maximum deformation from the 406% strain shown by the PP00 sample to about 3% shown by the strengthened PP30 sample with 30 wt % PAn-*g*-SGF. The results also show that in general the presence of PAn-*g*-SGF increased the Young's modulus. There was also a slight increment in the UTS value as the concentration of PAn-*g*-SGF was increased, whereas the yield strength increased about twofold for the PP30-sample with respect to the PP00 sample.

From the tensile test, the fracture mechanism in the composites was elucidated by SEM observations. Figure 5 shows an SEM micrograph of the surface of iPP strengthened with 30 wt % PAn-*g*-SGF near the fractured region. It can be observed that PAn-*g*-SGF was randomly distributed within the matrix. The tensile direction was vertical, as indicated by the arrow. Note that the fracture path was perpendicular to the tensile stress and was mainly along the decohesioned PAn-*g*-SFG from the iPP matrix. Furthermore, the fracture path evolved by interconnecting the decohesioned and fractured fibers (see arrows). The inset in Figure 5 shows a detail of the fracture path following the interfaces between the PAn-*g*-SGF and the iPP matrix, which were decohesioned. There is also evidence of SGF fracture along the iPP fracture trajectory.

Figure 6 shows SEM micrographs of the fractured surfaces for each sample. A ductile fracture mode was observed in the unreinforced PP00 sample; the surface was free of PAn-*g*-SGF and cavities. On the other hand, for the reinforced samples PP10, PP20, and PP30, the fracture mode was mainly brittle. The difference in the PAn-*g*-SGF concentration was evident from the images. The main characteristic shown is the PAn-*g*-SGF exposure, which is due to decohesion and fracture of the fibers during the tensile test. The interrelationship between these features helps to explain the mechanism of the brittle fracture.

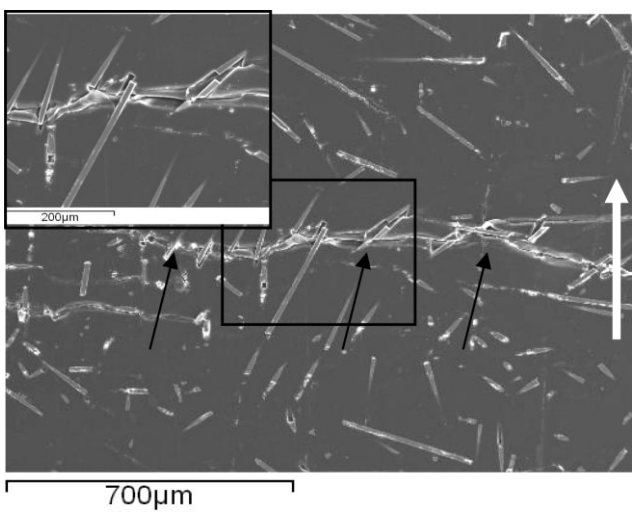

Figure 5 Fracture path on reinforced PP with 30 wt % PAn-*g*-SGF after deformation in the uniaxial deformation mode.

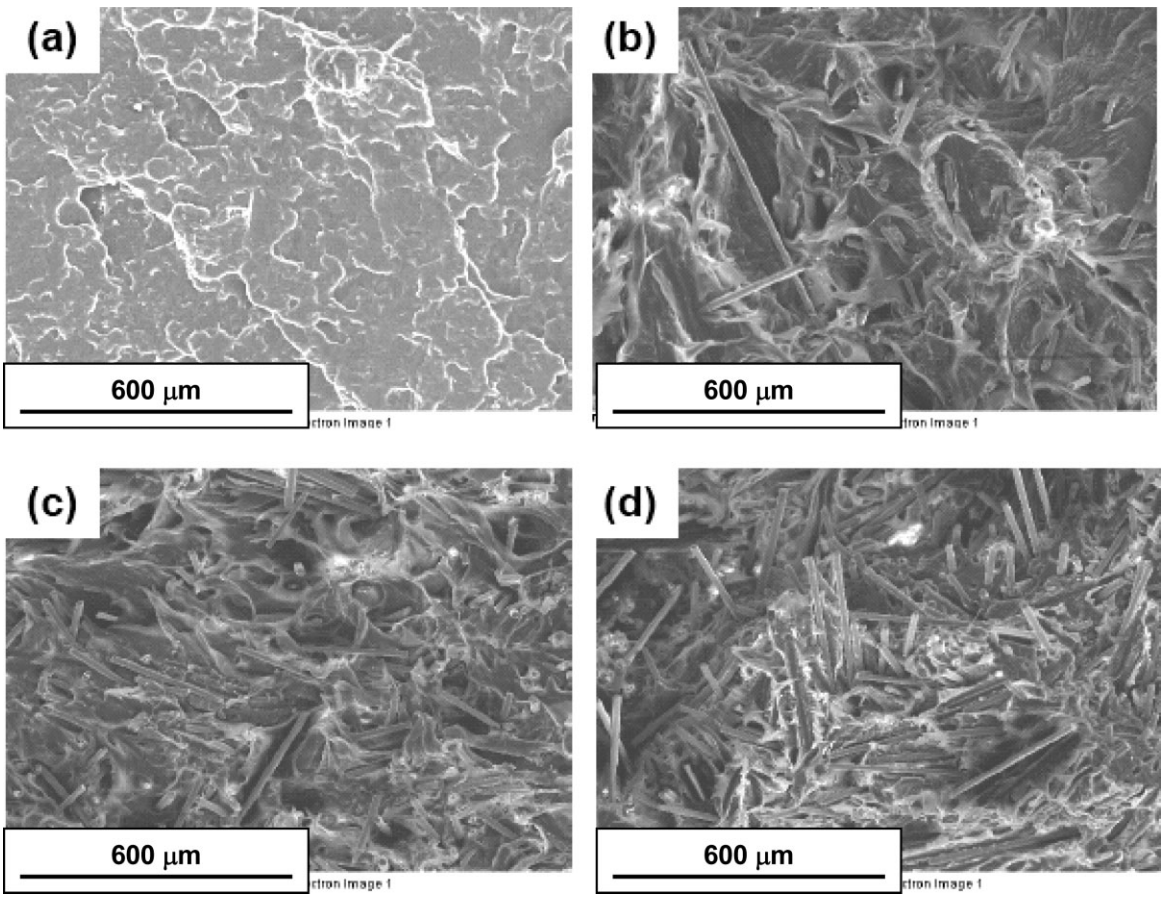

Figure 6 SEM micrographs of the fractured surfaces of (a) neat PP and (b–d) composites containing 10, 20, or 30 wt % PAn-*g*-SGF, respectively.

Usually, semicrystalline polymers are regarded as two-phase systems in which two components of different mechanical properties are appropriately combined.[17] Thus, fracture will always occur in the more fragile phase. The fracture of iPP/PAn-*g*-SGF, however, can be considered to a greater extent as elastic because of the higher degree of anisotropy and plastic deformation. The PAn-*g*-SGFs were randomly oriented and were subjected to tensile stress, and some of these fibers tended to orient along the stress direction when they were drawn. In this process, some separation may have occurred in the interface of the PAn-*g*-SGF and the iPP matrix, and depending on the bonding energy between the iPP and the PAn-*g*-SGF, it may or may not have induced chain slippage and failure.

In the case of the highest PAn-*g*-SGF content, it was more difficult for chain slippage to occur. Under tension, the molecular chains deformed and tended to break and may have exhibited brittle fracture (see Fig. 6). When the stresses in tension were further increased, these chains broke, and when a certain level of stress was reached, it tended to create microvoids. Over time, these voids may have merged, eventually generating a fracture over the surface. These fractures were stress concentrators at which the cracks could propagate, breaking either molecular chains or intermolecular interactions at the tip.

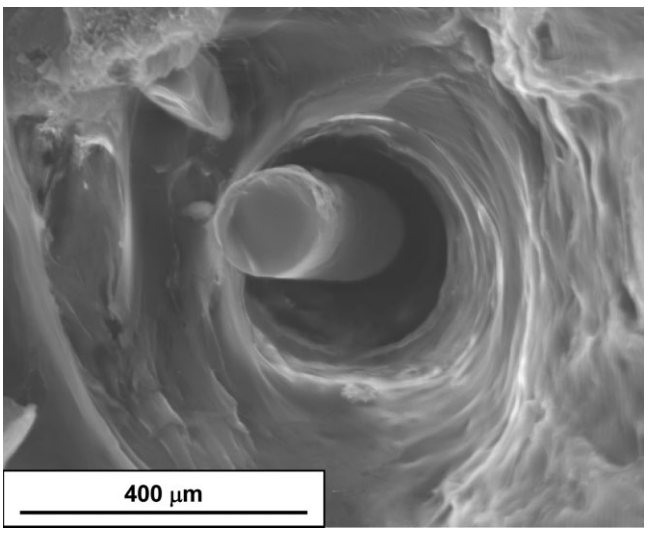

Figure 7 SEM micrograph showing the loss of adhesion between a single fiber and the polymer matrix. The fiber was fractured.

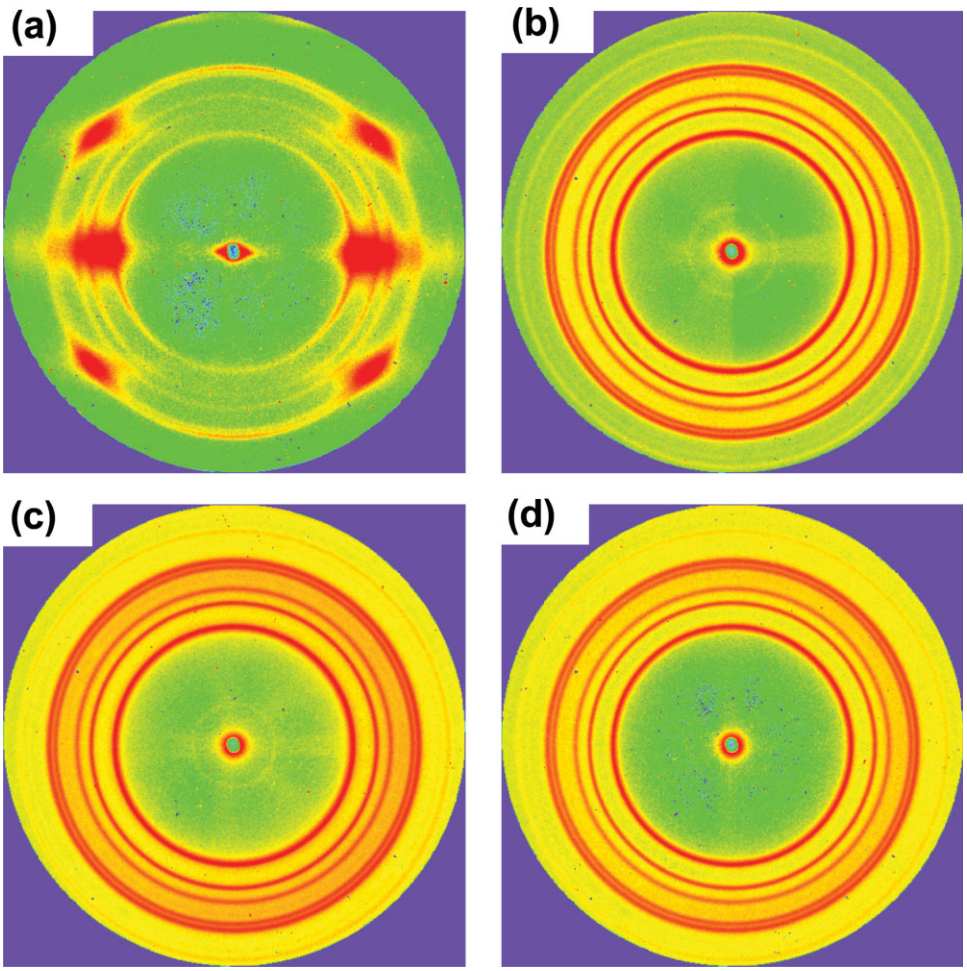

Figure 8 WAXS patterns of (a) neat PP after uniaxial elongation and (b–d) composites with 10, 20, or 30 wt % PAn-*g*-SGF, respectively. The patterns were obtained in the fractured region. [Color figure can be viewed in the online issue, which is available at www.interscience.wiley.com.]

The difference in behavior as the PAn-*g*-SGF concentration was varied is clear. As the concentration of the filler increased, the fracture mode tended to be more fragile, with less total deformation. Also, the density of the cavities increased at the interface of the fibers; this reduced the fiber interspaces and allowed fracture propagation. The fracture surfaces also showed that there was no fiber alignment during the tensile test, but the fibers were capable of inhibiting the slippage of iPP chains.

Figure 7 shows a detail of a great cavity formed under tensile stress in the iPP matrix and around a PAn-*g*-SGF. The cavity was associated with low bonding energy between the PAn-*g*-SGF and the iPP matrix. The micrograph shows complete decohesion between the fiber and the iPP matrix and brittle fracture in the tip of the fiber. The cavity formation may be due to the iPP being highly deformed locally, and it was only around the fiber where the iPP could slide.

The microstructure and possible macromolecular alignment in the fractured region of each sample were investigated via WAXS. It is widely documented that WAXS is an ideal technique for investigating the preferred orientation in macromolecules.[18,19] Figure 8(a–d) shows the corresponding diffraction patterns of iPP and the composites: the X-ray beam was directed at the tip of the fractured regions. The pattern of iPP is anisotropic, with well-defined and azimuthally concentrated equatorial reflections. The azimuthal concentration of the intensity indicates the alignment of the macromolecules along the tensile axis (vertical on the page). On the other hand, the X-ray patterns of the fractured composites appear isotropic. Azimuthal scans around the main interchain reflection in Figure 9(a) show intense and azimuthally narrow reflections for the iPP stretched sample. The intensity maxima are located at azimuthal angle (ϕ) values of 0 and 180°, confirming the macromolecular alignment along the tensile axis. On the other hand, the azimuthal scans for the fractured composites [PP10, PP20, and PP30; overlapping traces, Fig. 9(b)] showed a relatively constant intensity around the azimuth, confirming

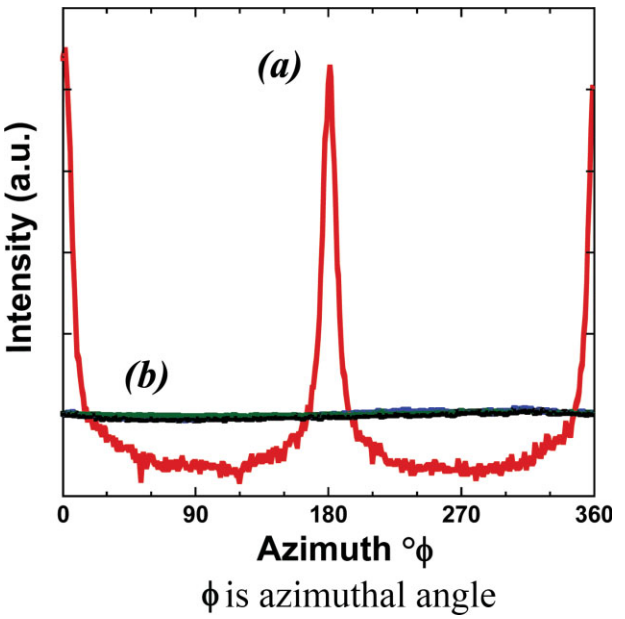

Figure 9 ϕ is azimuthal angle. Azimuthal intensity scans around the azimuth and through the main interchain reflections of (a) iPP and (b) iPP/PAn-*g*-SGF composites with 10, 20, or 30 wt % PAn-*g*-SGF. [Color figure can be viewed in the online issue, which is available at www.interscience.wiley.com.]

that the fractured composites remained isotropic. The results demonstrate that there was negligible (if any) macromolecular orientation under the action of tensile stress in the composites. In agreement with the SEM results discussed previously, the X-ray diffraction analyses also suggest that the poor adhesion between the PAn-*g*-SGF and the iPP matrix prevented any molecular alignment along the tensile axis.

CONCLUSIONS

Tensile uniaxial deformation experiments for iPP reinforced with PAn-*g*-SGF showed that the filler PAn-*g*-SGF indeed enhanced the mechanical properties (i.e., Young's modulus and yield stress) of iPP. The composite with the best mechanical properties (PP30) had an electrical conductivity lying in the range desired for its use as a dissipative material for ESD shielding, as shown in a previous report.[13] Uniaxial deformation showed that the failure in the composite arose from poor adhesion between the PAn-*g*-SGF and the iPP matrix, the PAn-*g*-SGF forming a path for the fracture's propagation through a percolation process. The material's failure was dominated by both SGF decohesion and polymeric chain rupture; therefore, the UTS was not influenced significantly by the amount of PAn-*g*-SGF.

The authors thank Patrick T. Mather (Syracuse University) and Wesley Burghardt (Northwestern University) for their support at the DuPont–Northwestern–Dow Collaborative Access Team Beamline 5, Advanced Photon Source, Argonne National Laboratory (Argonne, IL). The help of Mr. Anselmo González in machining the samples for mechanical testing is gratefully acknowledged.

References

1. Taipalus, R.; Harmia, T.; Friedrich, K. Appl Compos Mater 1999, 6, 167.
2. Taipalus, R.; Harmia, T.; Friedrich, K. Polym Compos 2000, 21, 396.
3. Faez, R.; Martin, I. M.; De Paoli, M. A.; Rezende, M. C. J Appl Polym Sci 2002, 83, 1568.
4. Jia, W.; Tchoudakov, R.; Segal; E.; Joseph, R.; Narkis, M.; Siegmann, A. Synth Met 2003, 132, 269.
5. Jia, W.; Tchoudakov, R.; Segal, E.; Joseph, R.; Narkis, M.; Siegmann, A. J Appl Polym Sci 2004, 91, 1329.
6. Barra, G. M. O.; Jacques, L. V.; Orefice, R. L.; Carneiro, J. R. G. Eur Polym J 2004, 40, 2017.
7. Jing, X.; Wang, Y.; Zhang, B. J Appl Polym Sci 2005, 98, 2149.
8. Malinauskas, A. Polymer 2001, 42, 3957.
9. Wu, C. G.; Chen, J. Y. Chem Mater 1997, 9, 399.
10. Wu, C. G.; Yeh, Y. R.; Chen, J. Y.; Chiou, Y. H. Polymer 2001, 42, 2877.
11. Li, Z. F.; Ruckenstein, E. Colloid J Interface Sci 2002, 251, 343.
12. Cruz-Silva, R.; Romero-Garcia, J.; Vazquez-Rodriguez, S.; Angulo-Sanchez, J. L. J Appl Polym Sci 2007, 105, 2387.
13. Cruz-Silva, R.; Romero-García, J.; Angulo-Sanchez, J. L. J Mater Sci 2005, 40, 5107.
14. Romero-Guzmán, M. E.; Romo-Uribe, A.; Cruz-Silva, R.; González, A. E. J Appl Polym Sci 2008, 109, 2207.
15. ASTM Standard D 638-03: Tensile Properties of Plastics; American Society for Testing and Materials: West Conshohocken, PA, 2003.
16. Kausch, H. H. Crazing in Polymers; Advances in Polymer Science; Springer-Verlag: Berlin, 1990, 52/53.
17. Kinloch, A. J.; Young, R. Fracture Behaviour of Polymers; Applied Science: London, 1984.
18. Alexander, L. E. X-Ray Diffraction Methods in Polymer Science; Wiley: London, 1969.
19. Windle, A. H. In Developments in Oriented Polymers; Ward, I. M., Ed.; Elsevier Applied Science: London, 1982; p 1.